Generation of Power-Efficient FCC-Compliant UWB Waveforms Using FBGs: Analysis and Experiment

Mohammad Abtahi, *Member, IEEE*, Julien Magné, Mehrdad Mirshafiei, Leslie A. Rusch, *Senior Member, IEEE*, and Sophie LaRochelle, *Member, IEEE, Member, OSA*

***Abstract*—In this paper, we design, analyze, and demonstrate experimentally U.S. Federal Communications Commission (FCC)-compliant power-efficient ultrawideband (UWB) waveforms generated by optical pulse shaping. The time-domain pulse shape is written in the frequency domain, and a single-mode fiber performs the frequency-to-time conversion. The waveform is inscribed in the frequency domain by the fiber Bragg grating (FBG). A significant challenge for this approach is elimination of an unwanted, positive rectangular pulse superimposed on the desired waveform. Our innovative use of balanced photodetection eliminates this pedestal, assuring compliance with the FCC mask at low frequency. Three UWB pulses with duration of 0.3, 0.6, and 1.2 ns are designed and tested experimentally. Whereas an excellent match between the optimized and measured pulses is achieved for the simpler, shorter duration waveforms, the noise in the fabrication process of FBGs limits the generation of the more complex, longer duration waveforms.**

***Index Terms*—Balanced detection, fiber Bragg grating (FBG), frequency-to-time conversion, microwave photonics, optical signal processing, pulse shaping, ultrawideband (UWB).**

I. Introduction

ULTRAWIDEBAND (UWB) radio has recently received tremendous attention for a wide variety of commercial applications such as wireless personal area networks, sensor networks, imaging systems, precision navigation, vehicular radar systems, medical monitoring, surveillance, and so on. UWB is attractive due to characteristics such as its ability to overlay existing band occupants without interfering, the potential for very high data rates, its high temporal resolution, the capability to penetrate through the obstacles and potentially small size [1].

In 2002, the U.S. Federal Communications Commission (FCC) approved an enormous unlicensed frequency band for UWB radio with the radiated power limited by a spectral mask [2]. UWB systems are highly power limited due to this mask, compared to more conventional (narrowband) systems. Pulse-shaping techniques that eke out the greatest legally allowed transmission power are critical to enhancing UWB performance. Various electrical and optical pulse generator architectures have been proposed; most focused on the widely adopted Gaussian, monocycle, and doublet pulses [3]–[10].

Two approaches exist for electronic pulse-based transmitters: a baseband pulse is up-converted to a center frequency in the UWB band by mixing with a local oscillator, or a pulse is generated that falls directly in the UWB band without frequency translation. In either case, a baseband impulse may excite a filter that shapes the pulse, or the pulse may be directly synthesized at radio frequency (RF) with no additional filtering [3]. For instance, a near Gaussian pulse is shaped from a triangular input signal and up-converted to a 528-MHz-wide channel in the 3.1–10.6-GHz UWB band [3]. Pulse shaping is integrated into the mixer, performing up-conversion, and shaping in one circuit. In [4], an overall design of pulse generator and transmit antenna is proposed. They designed a chip to generate Gaussian monocycle pulses with pulse position modulation (PPM) modulation. The minimum attainable pulse width is about 375 ps, with 330 ps offset for pulse-position modulation. In another technique, a single-chip complementary metal–oxide–semiconductor (CMOS) pulse generator with pulse shaping is proposed that combines various delayed pulses to form a short pulse that is filtered to obtain the UWB pulse [5]. A separate bandpass filter (3.1–5 GHz) is used to obtain an FCC-compliant pulse with duration of about 1.5 ns; the generated pulse is, however, not power efficient.

Optical pulse generation techniques for UWB have also been proposed based on optical spectral shaping and frequency-to-time conversion [6]–[9], a principle first established in [11]. The general concept of this technique is depicted in Fig. 1, where the spectrum of a broadband coherent source (BBS), typically a mode-locked laser, is shaped to match the desired time-domain waveform. The spectral shape is converted to a time-domain shape (a pulse shape) by passing through a dispersive medium such as dispersive fiber or a reflection chirped fiber Bragg grating (FBG) [12].

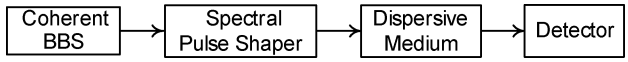

Fig. 1. Concept of arbitrary pulse generation by spectral pulse shaping.

The pulse shaping device in [13] is a 4-f grating and lens apparatus consists of two free space bulky gratings, two large focal length lenses to angularly disperse the frequency components, and a spatial light modulator (SLM) to modulate the amplitude of frequency components. The reflection type of this device is used in [6], where SLM is replaced by a single-layer

Manuscript received July 26, 2007; revised November 29, 2007. This work was supported in part by the TELUS Corporation and the Canadian Natural Science and Engineering Research Council. This work was presented in part at the 2007 European Conference on Optical Communications (ECOC).

M. Abtahi, M. Mirshafiei, L. A. Rusch, and S. LaRochelle are with the Center for Optics, Photonics and Laser (COPL), Electrical and Computer Engineering Department, Université Laval, Québec, QC G1V0A6 Canada (e-mail: abtahi@gel.ulaval.ca; mehrdad.mirshafiei.1@ulaval.ca; rusch@gel.ulaval.ca; larochel@gel.ulaval.ca).

J. Magné was with the Center for Optics, Photonics and Laser (COPL), Electrical and Computer Engineering Department, Université Laval, Québec, QC G1V0A6 Canada. He is now with the ITF Laboratories, Montréal, QC H4N 2G7, Canada (e-mail: magne@gel.ulaval.ca).

Color versions of one or more of the figures in this paper are available online at http://ieeexplore.ieee.org.

Digital Object Identifier 10.1109/JLT.2007.916586

liquid crystal modulator (LCM). Although these arbitrary waveform generators offer tremendous flexibility, and could generate the desired UWB pulse, they cannot be used in many applications due to their large size and high optical loss.

Following the general concept in Fig. 1, an all-fiber pulse shaper was recently proposed in [9] in which two optical filters with complementary spectra were placed in two arms of an interferometer to shape the power spectrum to a Gaussian monocycle or doublet pulse. The generated pulses, however, do not resemble the desired waveform, and the RF spectrums contain non-FCC-compliant baseband spectral content below 1 GHz. In addition, the interferometric structure of this pulse shaper leads to sensitivity to environmental changes such as temperature or vibration.

In another approach [10], a femtosecond pulse laser is spectrum sliced to the required pulse width. The optical pulse train is then injected into a nonlinear fiber, together with a continuous-wave (CW) probe laser, to create cross-phase modulation. An FBG is used as a frequency discriminator. By locating the probe laser at the linear or the quadrature slopes of the FBG reflection spectrum, UWB monocycle or doublet pulses are generated. The two laser sources used in this technique make it complex and costly. More importantly, additional electrical filtering is required to remove the noncompliant spectral content below 1.6 GHz.

We propose a new approach to generate UWB pulses that is both FCC compliant and maximizes the transmitted power. Our technique is also of the form shown in Fig. 1, with an FBG for pulse shaping. A length of single-mode fiber (SMF) disperses the signal to achieve the frequency-to-time conversion. One of the major challenges of spectral pulse-shaping techniques is the strictly positive mapping of optical intensity to electrical voltage [7]. Mathematically, this mapping is the equivalent of the desired (positive and negative going) pulse being superimposed on a positive rectangular pulse, a so-called pedestal. This characteristic creates nonnegligible spectral content near direct current (dc), and also spectral broadening (leakage) due to time windowing. The spectral content near dc can be seen in results reported in [6]–[9], [12], [13]. Our novel use of a two-arm structure and balanced photodetection allows us to easily remove the unwanted pedestal, and achieve a desired signal that has both positive and negative going parts.

We avoid the use of an interferometeric setup (as used in [9]) and take advantage of all-fiber components that are less sensitive to environmental perturbations: ours involves optical intensity-to-voltage conversion by the BPD before electronic subtraction, while an interferometric structure combines optical fields and is thus sensitive to optical phase variations easily induced by environmental changes.

The main advantage of the waveform generators in [6] and [13] is the reprogrammability of pulse-shaping filters (SLM or LCM) which makes it possible to generate all desired UWB waveforms. The reprogrammability in [10] is provided by varying the probe laser wavelength which enables the generation of either monocycle or doublet pulses. Our approach requires a new FBG if the UWB pulse is to be modified. A programmable version of our pulse generation allows tuning to one of three pulses (monocycle, doublet, or FCC compliant) [14]. The setup described in this paper is modified to exploit two FBG filters with overlapping spectra instead of a single pulse-shaping FBG. By tuning the cutoff wavelengths of the two FBG filters via stretching, the monocycle, doublet, or a simple FCC-compliant waveforms are generated.

In this paper, we present the steps involved in the design, simulation, and implementation of the UWB pulse generator. We exploit pulse design techniques proposed in [15], [16] to design various pulse shapes with maximum transmitted power (i.e., maximum spectral efficiency), while respecting the FCC mask. Three FCC-compliant pulses with durations of 0.3, 0.6, and 1.2 ns are designed, fabricated, and tested experimentally. Whereas an excellent match between the designed and measured pulses is observed for the shorter duration waveforms, the noise in the fabrication process of FBGs limits the generation of the more complex, longer waveforms.

The remainder of this paper is organized as follows. In Section II, we describe optimal FCC-compliant UWB waveform design and compare the spectral efficiency of various pulses. Section III presents the principle of operation of the proposed technique, as well as theoretical analysis and simulation. The experimental results and discussions are provided in Section IV. Finally, we conclude this paper in Section V.

II. Optimal UWB Waveform Design

As mentioned previously, the FCC requires that the equivalent isotropic radiated power (EIRP) spectra emitted by UWB transmit antennas adhere to the published spectral mask [2]. By sacrificing power efficiency, the FCC spectral mask can be respected for any pulse shape by simply reducing the average transmitted power. Recall UWB signals are highly power limited, thus a reduction in transmitted power greatly degrades performance. Ideally, the pulse should be designed to respect and efficiently exploit the FCC frequency mask. To this end, we follow the approach in [16], designing the optical pulse per

$$p(t) = \sum_{n=0}^{L-1} w[n]\, g(t - nT_0) \tag{1}$$

where $w[n]$ are L real coefficients, pulse spacing is T_0, and $g(t) = At\exp(-2(t/\tau_g)^2)$ is the Gaussian monocycle. The time between the maximum and minimum values of $g(t)$ is τ_g, and A is a scaling constant.

By fixing T_0, the real coefficients $w[n]$ can be determined numerically using an optimization process to maximize the average total power $P_{ave} = \int_0^{\omega_{\max}} |P(\omega)|^2 d\omega$, where $P(\omega)$ represents Fourier transform of $p(t)$ and $F_{\max} = \omega_{\max}/2\pi$ is the maximum frequency of interest (14 GHz, in our design). We transform the optimization problem to a set of linear equations that can be solved by SeDuMi Matlab optimization toolbox to provide the discrete autocorrelation function of the optimized tap coefficients [17]. We then use the spectral factorization method to obtain the required tap coefficients in (1) [18]. When the number of coefficients L is low, the spectrum of the designed pulse cannot follow the FCC mask, and the average transmitted power should be decreased to achieve compliance. By increasing the pulse length (or, equivalently, L), the spectrum of the pulse better fits the mask, and the spectral utilization

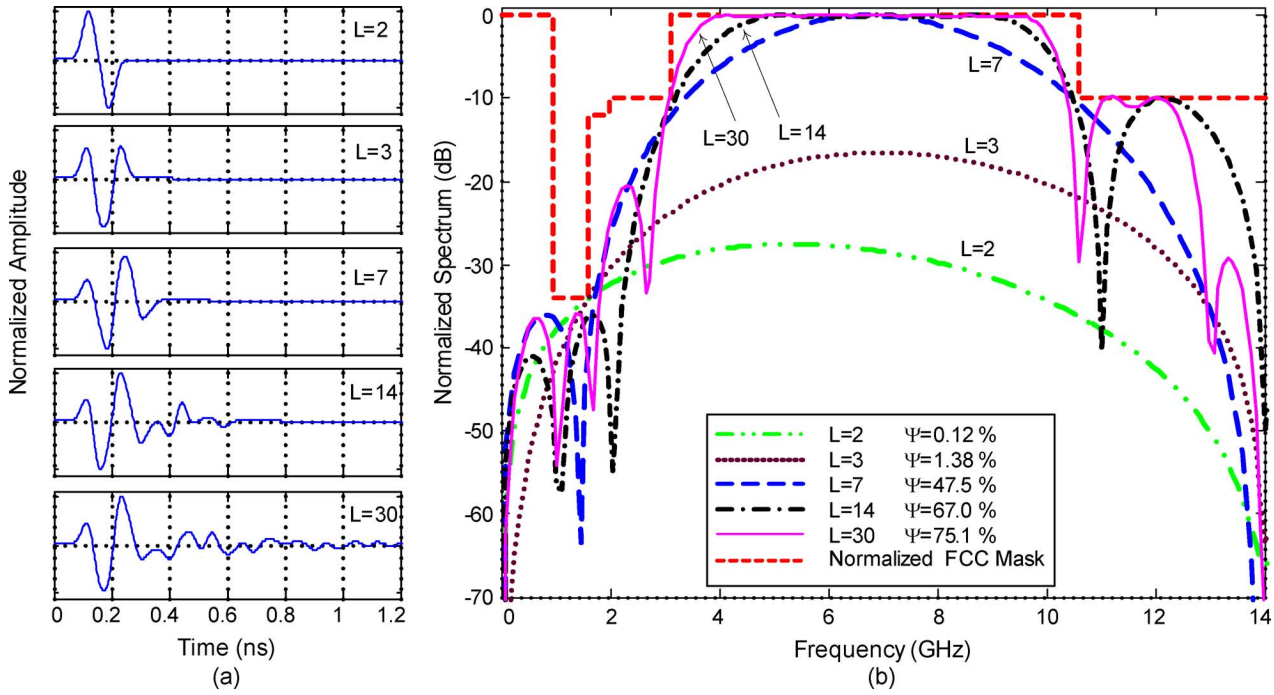

Fig. 2. Optimal UWB pulse shapes for (a) $L = 2, 3, 7, 14$ and 30 and (b) the corresponding spectra. The curves are normalized in order to respect the FCC spectral mask.

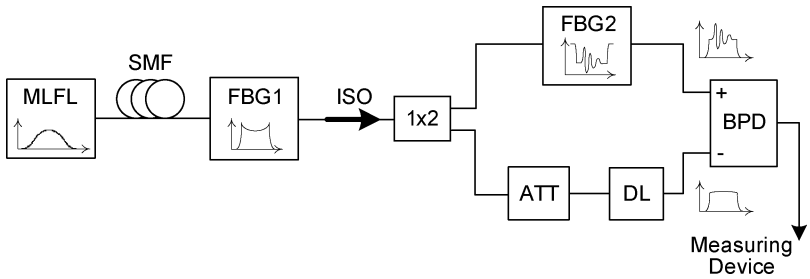

Fig. 3. Block diagram of the UWB waveform generator.

factor or spectral efficiency increases. The spectral efficiency $\Psi = \int_0^{\omega_{\max}} |P(\omega)|^2 d\omega / \int_0^{\omega_{\max}} S_{\mathrm{FCC}}(\omega)\, d\omega$ is the average power of pulse normalized by the total admissible power under $S_{\mathrm{FCC}}(\omega)$, the FCC mask. The larger the number of taps, the higher the spectral efficiency is; on the other hand, the longer the pulse, the more complex the shape is, requiring higher resolution in the FBG writing process.

The optimal designed pulses for $L = 2, 3, 7, 14,$ and 30 are plotted in Fig. 2(a). We used $T_0 = 35.7$ and $\tau_g = 46.5$ ps. The corresponding spectra of the pulses, normalized to their maximum value, are shown in Fig. 2(b). For $L = 2$ and 3, an extra reduction of 27.51 and 16.5 dB is required, respectively, to prevent violation of the FCC spectral mask. This is the main reason for low Ψ in the cases of $L = 2$ (0.12%) and $L = 3$ (1.38%). By increasing L, spectral efficiency increases to 47.5, 67 and 75.1% for $L = 7, 14$ and 30, respectively.

III. UWB Pulse Shaping

A. Principle of Operation

We use the general concept as in Fig. 1 to generate the optimally designed pulse in the previous section. A mode-locked fiber laser (MLFL) with large full-width at half-maximum (FWHM) bandwidth is used as a coherent broadband source. The spectral pulse shaper in our design is an FBG in transmission with a transfer function proportional to the desired pulse. We use an appropriate length of SMF as the dispersive medium to generate the total required dispersion for the frequency-to-time conversion.

The particular form of our embodiment is heavily influenced by the requirement to remove the undesired superimposed rectangular pulses imprinted on the desired pulse during conversion to the time domain. Recall that all pulses generated by optical pulse-shaping techniques using frequency-to-time conversion contain an unwanted additive rectangular pulse superimposed on the desired pulse shape, leading to strong, unwanted spectral components in low frequencies ($<\sim$ 1 GHz) that cannot be removed by a dc block. We use a balanced photodetector (BPD) to completely remove unwanted low-frequency components. The block diagram of our proposed technique is shown in Fig. 3. FBG1 is used to flatten the mode-locked source spectrum over the desired bandwidth. The optical signal is then divided into two arms. In the first arm, we use a second chirped grating FBG2 with a complex apodization profile optimized to imprint

the desired pulse shape on the spectrum of the source. In the second arm, the optical delay line (DL) and the variable attenuator (ATT) are used to balance the amplitude and the delay of the two arms. We used an isolator to prevent back and forth reflections between the two FBGs. The SMF may be placed anywhere along the generator; placing it before spectral shaping avoids requiring SMF in both arms of the BPD.

B. Theoretical Analysis and Simulation

The functionality of each component in Fig. 3 can be modeled by a transfer function in order to simulate the generated pulse shape at the BPD output. The PSD of the passive MLFL can be approximated by

$$A_S(\omega) = \operatorname{sech}^2\left(a\left(\omega - \omega_0\right)\right) \tag{2}$$

where ω and ω_0 are the angular and the centre frequencies, respectively, and a is a constant. Neglecting the propagation delay of the pulse envelope, the transfer function of a lossless dispersive SMF can be modeled with very good precision [19] by

$$H_{\mathrm{SMF}}(\omega) = \exp\left\{-jL_f\left(\frac{\beta_2}{2}(\omega-\omega_0)^2 + \frac{\beta_3}{6}(\omega-\omega_0)^3\right)\right\} \tag{3}$$

where L_f is the fiber length. Also, $\beta_2 = d^2\beta(\omega)/d\omega^2\big|_{\omega=\omega_0}$ and $\beta_3 = d^3\beta(\omega)/d\omega^3\big|_{\omega=\omega_0}$ are known as the second- and third-order dispersion parameters and $\beta(\omega)$ is the mode propagation constant. β_2 (ps^2/km) is related to the dispersion parameter D (ps/km-nm) through $\beta_2 = -\lambda_0^2 D/2\pi c$ and β_3 (ps^3/km) is related to the dispersion slope D_P (ps/km-nm^2) by $\beta_3 = \left(\lambda_0^2/2\pi c\right)^2 D_P$. The center wavelength is $\lambda_0 = 2\pi c/\omega_0$ and c is the light speed. For typical SMF, D_P is very small and thus third-order chromatic dispersion is negligible over short distances and for narrow bandwidths. In the present case, we assume that the fiber group delay is linear over the frequency band of interest.

Referring again to Fig. 3, FBG1 is used to flatten the source spectrum, therefore, its ideal transfer function is

$$H_{\mathrm{FBG1}}(\omega)\big|_{\mathrm{ideal}} = \begin{cases} \dfrac{1}{A_S(\omega)}, & \omega \in \left(\omega_c - \dfrac{\Delta\omega}{2}, \omega_c + \dfrac{\Delta\omega}{2}\right) \\ 0, & \text{otherwise} \end{cases} \tag{4}$$

where $\Delta\omega$ is the desired bandwidth around ω_c.

Of course, a real FBG cannot follow exactly the desired profile in (4). The error between the target spectral profile defined in (4) and the fabricated FBG1 spectral response should be minimized by choosing an appropriate apodization profile. In general, finding the apodization profile of a grating operating in transmission is a relatively easy task, as long as the target spectral profile does not vary too rapidly. The chirped grating's spectral response $T(\lambda)$ and the apodization profile is typically related by [20]

$$\Delta n_{ac}(\lambda) = \frac{n_{\mathrm{eff}}}{\Gamma\pi}\sqrt{-2\ln\left(T(\lambda)\right) C_m}. \tag{5}$$

This equation links the index modulation amplitude $\Delta n_{ac}(\lambda)$ to the desired transmission profile $T(\lambda)$ for FBG1. In (5), C_m is the index modulation chirp, n_{eff} is the effective refractive index, and Γ is the ratio of modal power that overlaps with the grating (Γ is the confinement factor if the grating is confined in the fiber core). Once the apodization profile is obtained, we simulate the grating spectral response using a standard transfer matrix method. This grating spectral response is then compared to the target response; slight modifications are made to the apodization profile to tune it to the target response. After several iterations, the apodization profile leading to the best spectral response is achieved.

The transfer function of FBG2 can be obtained by a time-to-frequency mapping of the designed UWB pulse shape $p(t)$. In this case, the pulse duration ΔT is mapped to the $\Delta\lambda$ linewidth corresponding to $\Delta\omega = 2\pi c\Delta\lambda/\lambda_0^2$, the desired bandwidth. The ratio $\Delta T/\Delta\lambda$ is equal to the total required dispersion of the fiber (i.e., $D \times L_f$) and determines the required length of SMF for converting the pulse to the time domain. The ideal transfer function of pulse shaping FBG2 can be expressed by

$$H_{\mathrm{FBG2}}(\omega)\big|_{\mathrm{ideal}} = 1 + \alpha\, p\left(\frac{2\pi c}{\omega}\right) \tag{6}$$

where α is a constant. As with FBG1, we use (5) and (6) to obtain the apodization profile and simulate the transfer function by the transfer matrix method. The Fourier transform of the optical signals at the inputs to the balanced photodetector can be expressed by

$$E_1(\omega) = \alpha_1\, A_S(\omega) H_{\mathrm{SMF}}(\omega) H_{\mathrm{FBG1}}(\omega) H_{\mathrm{FBG2}}(\omega) \tag{7-a}$$

$$E_2(\omega) = \alpha_2 A_S(\omega) H_{\mathrm{SMF}}(\omega) H_{\mathrm{FBG1}}(\omega) e^{-j\omega\tau} \tag{7-b}$$

where α_1 represents the total loss in the first arm, and α_2 can be adjusted by variable attenuator to balance the power in the two arms. A variable delay τ in the second arm compensates for any delay between these two lines. Finally, the detected signal at the output of the balanced photodetector is

$$e_{\mathrm{out}}(t) = |e_1(t)|^2 - |e_2(t)|^2 \tag{8}$$

where $e_i(t) = \mathrm{IFT}\{E_i(\omega)\}$, $i = 1, 2$. We supposed that the BPD has a flat transfer function over the signal bandwidth.

We now examine our pulse-shaping strategy via simulation. The spectrum of the broadband source is measured and curve fitted. This fitted curve is used to design the apodization profile of FBG1, whose role is to carve out the desired wavelength band, and compensate for the nonflat spectrum of the broadband source. The simulated transmittivity of FBG1 is given by the dotted line in Fig. 4(a). Kinks in this curve are the result of a finite duration apodization profile. FBG2 was designed to realize the optimized pulse shape when $L = 14$ taps are used in (1). The simulated transmittivity of FBG2 is given by the solid line in Fig. 4(a). The simulated spectra of the output of FBG1 using the fitted curve for the broadband source spectra as input is given by the dashed line in Fig. 4(b). We see ringing at the cutoff wavelengths. Subsequent filtering by FBG2 yields the spectra given by the solid line in Fig. 4(b). We see the ringing of FBG1 now imprinted on the output of FBG2. We now add 5.46 km of SMF with 16.3-ns/km/nm dispersion to our simulator, and examine the electrical output from each of the photodetectors in the balanced photodetector. Fig. 4(c) gives time traces for the output of the photodetectors in the upper and lower arms. In

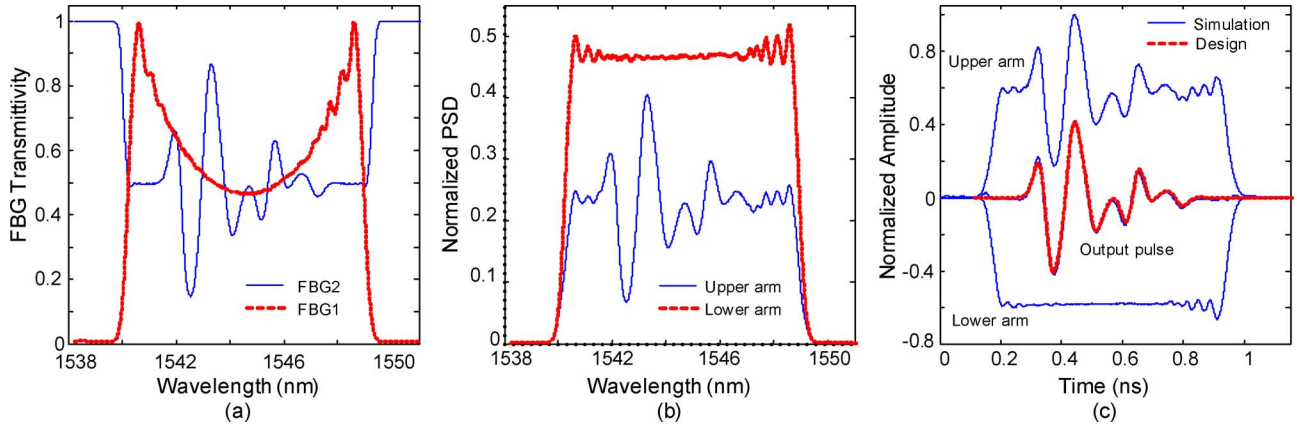

Fig. 4. Simulation results for $L = 14$. (a) Transmittivity of FBGs. (b) PSD at upper and lower arms. (c) Simulated and designed output pulse.

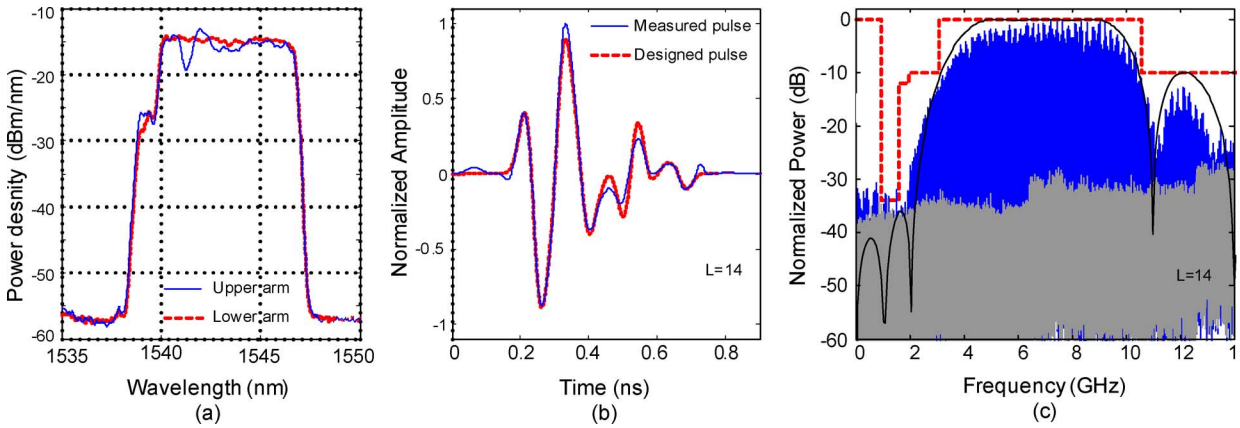

Fig. 5. Experimental results for $L = 14$. (a) PSD at upper and lower arms. (b) Measured UWB pulse. (c) Spectrum.

the upper arm, we have the desired pulse shape plus the undesired rectangular pedestal; note the ringing near the pulse edges. In the lower arm, we have the rectangular pedestal alone; note again the ringing. The output of the balanced photodetector is also shown in Fig. 4(c). By subtracting the lower arm from the upper arm, the vast majority of the ringing has been eliminated. In this plot, we have superimposed the final result of our simulation (solid line) with the target optimized pulse in a dashed line.

IV. Experiment and Discussions

The block diagram of the setup is very similar to Fig. 3. We used an MLFL fabricated in our lab based on the general concept in [21]. The MLFL generates 270 fs sech^2 pulses with a repetition rate of 31.25 MHz. As in the simulation, we used 5.46 km of SMF with a measured dispersion of 16.3 ns/km/nm. We used an EDFA after the SMF to provide more optical power at the BPD inputs and thus increase the detected signal power over the noise floor of the detector and measuring devices. As the EDFA has nonflat gain, we measured the optical PSD after the EDFA and fabricated FBG1 with an apodization profile to flatten the amplified mode-locked source spectrum over $\sim$ 7.5-nm bandwidth.

We fabricated the FBGs using a standard phase mask scanning technique with a 244-nm ultraviolet (UV) beam. For FBG1, we used a 14-cm mask with a chirp rate of 2.5 nm/cm and a H2-loaded photosensitive specialty fiber. The grating apodization was performed phase-mask dithering during the UV scan. The measured spectral response of the grating differs from the predicted response via numerical simulation because of fabrication errors due to phase mask imperfections, nonuniformities in fiber photosensitivity, and cladding mode coupling.

FBG2 was fabricated with a phase mask with a chirp rate of 0.498 nm/cm. Both fiber gratings described in this paper are linearly chirped gratings operated in transmission. We focused on the generation of the UWB pulse with $L = 14$, however, as we will explain later, we repeated the experiment for $L = 7$ and 30 with minor modification to our setup.

The power spectral density (PSD) incident on each photodetector in the BPD is shown in Fig. 5(a); the solid line represents the PSD after FBG2 in the upper arm and the dashed line represents the PSD after DL in the lower arm. The optical spectra are measured by an optical spectrum analyzer (OSA) with a resolution of 0.1 nm (ANDO AQ6317B). The power spectral density at the output of FBG1 is equal to the PSD of the lower arm [dashed line in Fig. 5(a)] except for a constant attenuation factor. As we expected, FBG1 cuts the source spectrum and compensates (flattens) source spectrum. The small variation from a flat spectrum is because of imperfections in the FBG writing process.

The two optical signals (upper and lower arms) are input to a 10-GHz DSC-710 BPD. The output UWB pulse shape

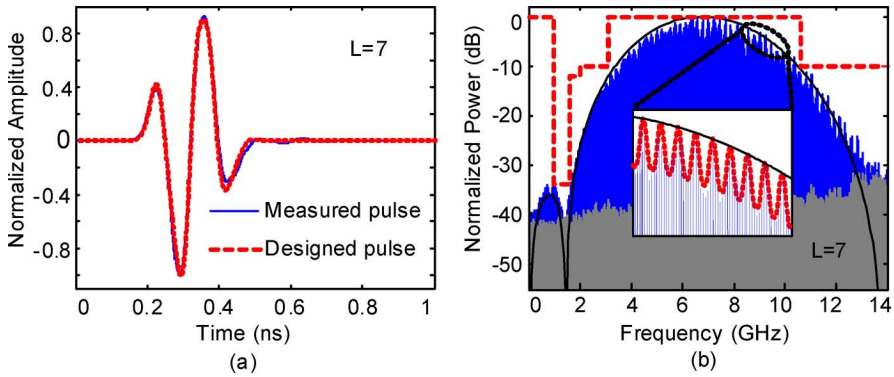

Fig. 6. Experimental results for $L = 7$. (a) Measured UWB pulse. (b) Spectrum. The enlarged part shows the sinusoidal variations due to multiple reflections.

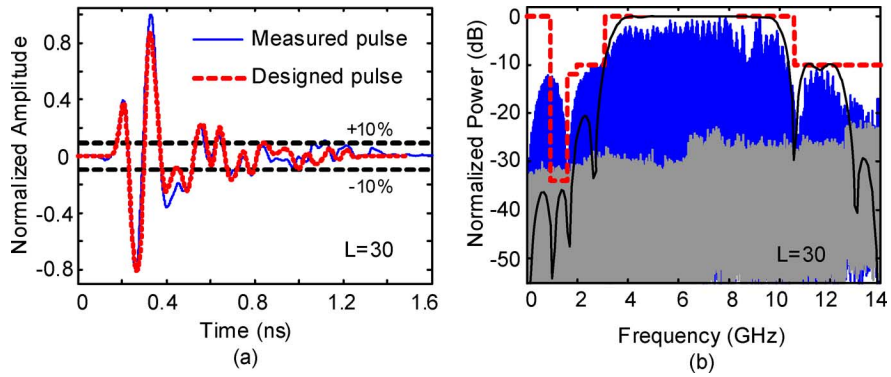

Fig. 7. Experimental results for $L = 30$. (a) Measured UWB pulse. (b) Spectrum.

[Fig. 5(b)] is then viewed by a 40-GHz sampling scope (Agilent 86100A) and its electrical power spectrum [Fig. 5(c)] is measured by a high-speed RF spectrum analyzer (HP 8565E). Comparing the designed pulse (dashed line) with the measured pulse (solid line) in Fig. 5(b), we see a good match, despite some modifications in the peaks attributable to imperfections in the FBG writing process and to the imperfect, bandlimited spectral response of the BPD. The measured peak-to-peak voltage is about 200 mv. The electrical PSD of the pulse in Fig. 5(c) scrupulously respects the FCC spectral mask (dashed line) and follows our design (solid line). The reduced power in frequencies above 10 GHz is mainly because of the frequency response of the BPD that inflicts more than 5 dB loss at 14 GHz compared to the dc level. The gray area in this figure represents the noise floor of the BPD and the RF spectrum analyzer. We note that the pulse has an almost flat spectrum in the 4–9-GHz range.

The experiment was repeated for the optimized UWB pulses with $L = 7$ and 30 taps as well, with some modifications. The pulse duration ΔT for $L = 7$ is almost half of the pulse duration for $L = 14$. Thus, we can either use half of the available source bandwidth, or decrease the mapping ratio $\Delta T/\Delta\lambda$ by a factor of 2. We chose to use half the available bandwidth by adding an optical filter to cut the upper half of the already flattened spectrum. We calculated the apodization profile for the $L = 7$ pulse shape and wrote another FBG2. The measured and target pulse are shown in Fig. 6(a); an excellent match can be observed. The spectrum of the pulse in Fig. 6(b) perfectly follows the designed spectrum (solid line) and respects the FCC mask. Waveforms with even simpler shape (e.g., Gaussian monocycle and doublet) could also be generated with high precision using this method.

A small part of the spectrum in Fig. 6(b) is enlarged in the inset to show the sinusoidal variation in the envelope of the measured spectrum. We attribute this variation to reflections of the pulse between the BPD and the RF spectrum analyzer due to impedance mismatch, and verified this hypothesis as follows. Let r be the reflection coefficient and τ_r the delay for each reflection. The measured spectrum can be modeled by $P_r(\omega) = P(\omega)(1 + re^{-j\omega\tau_r} + r^2e^{-j\omega 2\tau_r} + \cdots)$, where $P(\omega)$ is Fourier transform of the designed pulse. We assume only two reflections, and fit r and τ_r to our measurements. The spectrum predicted using two reflections is given by the dashed line in the inset, verifying the source of the variation as an impedance mismatch.

Our experiment for $L = 30$ showed that generation of more complex pulses requires higher precision in the FBG fabrication process. For $L = 30$, the pulse duration is doubled compared to the first design for $L = 14$. As the total available bandwidth is limited, we chose to increase the mapping ratio and use the same bandwidth as before. Therefore, the SMF length was increased for an appropriate frequency-to-time conversion, i.e., 10.56 km of SMF with total dispersion of 173.9 ps/nm. We fabricated another FBG2 for the pulse with $L = 30$, and present results in Fig. 7. By comparing the measured pulse with the designed pulse in Fig. 7(a), we observe an acceptable match in the first half of the pulse, but deviations in the second half are severe. During the FBG writing process, we observed signifi-

cant FBG fabrication noise when pulse amplitude went below 10% of the peak amplitude. At the same time, because our mapping ratio was doubled, the apodization profile includes a much greater number of swings for the same fixed phase mask length (and linewidth), also leading to greater deviation from the designed pulse in the form of overshoots. The measured electrical spectrum of the pulse [Fig. 7(b)] is not flat in the 3–9-GHz frequency range and contains large spectral content at low frequencies (< 2 GHz), violating the FCC spectral mask. This experiment demonstrates the practical limits (not theoretical) of the proposed method. A more precise fabrication device could reduce these limitations.

V. Conclusion

Gaussian monocycles and doublets are poorly adapted to the spectral mask imposed by the FCC. UWB communications systems are severely power limited due to regulatory constraints. Performance can be improved by maximizing transmit power via an FCC-compliant pulse that efficiently exploits the allowable power under the FCC mask. Electrical techniques for generation of such complex UWB pulses encounter many difficulties due to the extreme bandwidth of the pulse. In this paper, we designed, simulated, and experimentally demonstrated optical generation of the power-efficient, FCC-compliant UWB pulses using fiber Bragg gratings. Our approach is robust against environmental changes such as temperature or vibration compared to the interferometeric structure. Three FCC-compliant pulses with duration of 0.3, 0.6, and 1.2 ns and theoretical spectral efficiency of 47.5%, 67%, and 75.1%, respectively, are designed and demonstrated. An excellent match between the designed and measured pulses is observed for the first two waveforms, with spectrums scrupulously respecting the FCC spectral mask.

The generation of the more complex waveforms is limited by fabrication noise due to phase mask imperfections, nonuniformities in fiber photosensitivity and cladding mode coupling. Note that imperfections in the first (flattening) FBG are compensated by balanced detection that removes the small unwanted variations in the signal spectrum.

Acknowledgment

The authors would like to thank S. Doucet for many worthwhile discussions and help with FBG design.

References

[1] S. Roy, J. R. Foerster, V. S. Somayazulu, and D. G. Leeper, "Ultrawideband radio design: The promise of high-speed, short range wireless connectivity," *Proc. IEEE*, vol. 92, no. 2, pp. 295–311, Feb. 2004.

[2] "First report and order," U.S. Federal Communications Commission, 2002, revision of part 15 of the Commission's rules regarding ultrawideband transmission systems.

[3] D. D. Wentzloff and A. P. Chandrakasan, "Gaussian pulse generators for subbanded ultra-wideband transmitters," *IEEE Trans. Microw. Theory Tech.*, vol. 54, no. 4, pp. 1647–1655, Apr. 2006.

[4] S. Bagga, A. V. Vorobyov, S. A. Haddad, A. G. Yarovoy, W. A. Serdijn, and J. R. Long, "Co-design of an impulse generator and miniaturized antennas for IR-UWB," *IEEE Trans. Microw. Theory Tech.*, vol. 54, no. 4, pp. 1656–1666, Apr. 2006.

[5] L. Smaini, C. Tinella, D. Helal, C. Stoecklin, L. Chabert, C. Devaucelle, R. Cattenoz, N. Rinaldi, and D. Belot, "Single-chip CMOS pulse generator for UWB systems," *IEEE J. Solid-State Circuits*, vol. 41, no. 7, pp. 1551–1561, Jul. 2006.

[6] I. S. Lin, J. D. McKinney, and A. M. Weiner, "Photonic synthesis of broadband microwave arbitrary waveforms applicable to UWB communications," *IEEE Microw. Wireless Compon. Lett.*, vol. 5, no. 4, pp. 226–228, Apr. 2005.

[7] J. D. McKinncy, I. S. Lin, and A. M. Weiner, "Shaping the power spectrum of ultrawideband radio frequency signals," *IEEE Trans. Microw. Theory Tech.*, vol. 54, no. 12, pp. 4247–4255, Dec. 2006.

[8] B. Bortnik, I. Y. Poberezkskiy, J. Chou, B. Jalali, and H. R. Fetterman, "Predistortion technique for RF-photonic generation of high-power UWB arbitrary waveforms," *J. Lightw. Tech.*, vol. 24, no. 7, pp. 2752–2759, Jul. 2006.

[9] C. Wang, F. Zeng, and J. Yao, "All-fiber UWB pulse generation based on spectral shaping and dispersion-induced frequency-to-time conversion," *IEEE Photon. Technol. Lett.*, vol. 19, no. 3, pp. 137–139, Feb. 2007.

[10] F. Zeng, Q. Wang, and J. Yao, "All-optical UWB impulse generation based on cross-phase modulation and frequency discrimination," *Electron. Lett.*, vol. 43, no. 2, pp. 119–121, Jan. 2007.

[11] P. V. Kelkar, F. Coppinger, A. S. Bhushan, and B. Jalali, "Time-domain optical sensing," *Electron. Lett.*, vol. 35, no. 19, pp. 1661–1662, Sep. 1999.

[12] A. M. Weiner, "Femtosecond pulse shaping using spatial light modulators," *Rev. Sci. Instrum.*, vol. 71, no. 5, pp. 1929–1960, May 2000.

[13] J. Chou, Y. Han, and B. Jalali, "Adaptive RF-photonic arbitrary waveform generator," *IEEE Photon. Technol. Lett.*, vol. 15, no. 4, pp. 581–83, Apr. 2003.

[14] M. Abtahi, M. Mirshafiei, J. Magné, L. A. Rusch, and S. LaRochelle, "Ultra-wideband waveform generator based on optical pulse shaping and FBG tuning," *IEEE Photon. Technol. Lett.*, vol. 20, no. 2, pp. 135–137, Jan. 2008.

[15] X. Wu, Z. Tian, T. N. Davidson, and G. B. Giannakis, "Optimal waveform design for UWB radios," *IEEE Trans. Signal Process.*, vol. 45, no. 6, pp. 2009–2021, Jun. 2006.

[16] X. Luo, L. Yang, and G. B. Giannakis, "Designing optimal pulse-shapers for ultra-wideband radios," *J. Commun. Netw.*, vol. 5, no. 4, pp. 334–353, Dec. 2003.

[17] J. F. Strum, "Using SeDuMi 1.02, a Matlab Toolbox for optimization over symmetric cones," 1991 [Online]. Available: http://sedumi.mcmaster.ca

[18] S.-P. Wu, S. Boyd, and L. Vandenberghe, "FIR filter design via semidefinite programming and spectral factorization," in *Proc. 35th Conf. Decision Control*, Kobe, Japan, Dec. 1996, pp. 271–276.

[19] G. P. Agrawal, *Lightwave Technology: Telecommunication Systems*. New York: Wiley, 2005.

[20] S. Pereira and S. LaRochelle, "Field profiles and spectral properties of chirped Bragg grating Fabry-Perot interferometers," *Opt. Express*, vol. 13, pp. 1906–1915, Mar. 2005.

[21] H. A. Haus, K. Tamura, L. E. Nelson, and E. P. Ippen, "Stretched-pulse additive pulse mode-locking in fiber ring lasers: Theory and experiment," *IEEE J. Quantum Electron.*, vol. 31, no. 3, pp. 591–598, Mar. 1995.

Mohammad Abtahi (M'06) received the B.S. degree in electrical engineering from Shiraz University, Shiraz, Iran, in 1991, the M.S. degree from Sharif University of Technology (SUT), Tehran, Iran, in 1994, and the Ph.D. degree from both SUT and Institut National Polytechnique de Grenoble (INPG), Grenoble, France, in 2000.

From February 2001 to June 2005, he was with Iran Telecom Research Center (ITRC) as a Member of Technical Faculty (Assistant Professor) and Head of Wireless Communications Group. Currently, he is with the Centre d'optique, photonique et laser (COPL), Department of Electrical and Computer Engineering, Université Laval, Québec City, QC, Canada. His research interests are free-space optical communications, optical CDMA networks, and optical processing for ultrawideband systems.

Julien Magné received the B.S. degree in engineering optics from the Ecole Nationale Supérieure de Science Appliquée et Technologie (ENSSAT), Lannion, France, in 2001 and the M.Sc. and Ph.D. degrees in electrical engineering from Université Laval, Québec City, QC, Canada, in 2004 and 2007, respectively.

Currently, he is a Postdoctoral Member of Staff at ITF Laboratories, Montréal, QC, Canada. His research interests include high-power fiber lasers and amplifiers, mode-locked fiber lasers, fiber Bragg gratings, optical signal processing, and nonlinear optics.

Mehrdad Mirshafiei was born on April 20, 1984. He received the B.S. degree in electrical engineering from the School of Electrical and Computer Engineering, Tehran University, Tehran, Iran. Currently, he is working towards the M.Sc. degree in electrical engineering at the Centre d'optique, photonique et laser (COPL), Department of Electrical and Computer Engineering, Université Laval, Québec City, QC, Canada.

His research interest is optical processing for ultrawideband pulse shaping.

Leslie A. Rusch (S'91–M'94–SM'00) received the B.S.E.E. (honors) degree from the California Institute of Technology, Pasadena, in 1980 and the M.A. and Ph.D. degrees in electrical engineering from Princeton University, Princeton, NJ, in 1992 and 1994, respectively.

From 2001 to 2002, she was the Manager of a group researching new wireless technologies at Intel Corporation. Currently, she is a Full Professor at the Centre d'optique, photonique et laser (COPL), Department of Electrical and Computer Engineering, Université Laval, Québec City, QC, Canada, performing research in wireless and optical communications. Her research interests include optical-code-division multiple access using noncoherent sources for metropolitan area networks; semiconductor and erbium-doped optical amplifiers and their dynamics; and in wireless communications, high performance, reduced complexity receivers for ultrawideband systems employing code-division multiple access.

Sophie LaRochelle (M'00) received the B.S. degree in engineering physics from Université Laval, Québec City, QC, Canada, in 1987 and the Ph.D. degree in optics from the University of Arizona, Tucson, in 1992.

From 1992 to 1996, she was a Research Scientist at the Defense Research and Development Canada—Valcartier, where she worked on electrooptical systems. Currently, she is a Professor at the Centre d'optique, photonique et laser (COPL), Department of Electrical and Computer Engineering, Université Laval, , where she holds the Canada Research Chair in Optical Fibre Communications and Components. Her current research activities are focused on active and passive fiber optics components for optical communication systems including fiber Bragg gratings, optical amplifiers, and multiwavelength and pulsed fiber lasers. Other research interests include packet-switched networks with photonic code processing, transmission of radio-over-fiber signals and OCDMA.

Dr. LaRochelle is a member of Optical Society of America (OSA) and IEEE Lasers and Electro-Optics Society (LEOS).